Research Square

Preprints are preliminary reports that have not undergone peer review.
They should not be considered conclusive, used to inform clinical practice,
or referenced by the media as validated information.

Green-Function Analysis of Localized Rossby Wave Packets in β-Plane Flows

Albertus Sulaiman

albe002@brin.go.id

National Research and Innovation Agency

Research Article

Keywords: Localized Rossby wave packets, Green-function method, β-plane dynamics, Eddy viscosity, Multiscale asymptotics

Posted Date: September 7th, 2026

DOI: https://doi.org/10.21203/rs.3.rs-10500507/v1

License: This work is licensed under a Creative Commons Attribution 4.0 International License.
Read Full License

Additional Declarations: No competing interests reported.

Green-Function Analysis of Localized Rossby Wave Packets in β-Plane Flows

Albertus Sulaiman
Research Center for Climate and Atmosphere, Badan Riset dan Inovasi Nasional (BRIN), KST BJ Habibie, Tangerang Selatan, Banten, Indonesia
email: albe002@brin.go.id

Abstract

The dynamics of localized eddy and Rossby wave packets in weakly diffusive β-plane flows is investigated using multiscale asymptotic analysis and Green-function methods. Starting from the incompressible momentum equations with a Mellor-Yamada eddy-viscosity closure, we derive a reduced streamfunction equation in which vertical turbulent diffusion influences horizontal dynamics through a vertical eigenvalue problem. The leading-order solution is a localized Gaussian vortex, while higher-order corrections are obtained analytically via Green-function techniques. The analysis reveals a radius-dependent Rossby-wave dispersion relation, showing that the vortex radius sets a critical threshold separating eastward and westward packet propagation. The vertical eddy-viscosity coefficient modifies the vertical eigenstructure and thus controls the amplitude and evolution of the wave packet. First-order perturbations generate secondary vorticity structures and lateral energy scattering around the primary vortex, indicating a mechanism for redistributing energy from coherent eddies to surrounding flow structures. The results provide an analytically tractable description of the coupling between eddy viscosity, vortex dynamics, and localized Rossby-wave propagation in rotating geophysical flows.

Keywords: Localized Rossby wave packets; Green-function method; *β*-plane dynamics; Eddy viscosity; Multiscale asymptotics.

1. INTRODUCTION

Local vortex structures are common in rotating geophysical flows. They redistribute momentum and vorticity across many spatial and temporal scales. In the ocean and atmosphere, coherent vortices and Rossby wave disturbances form when planetary rotation, background flow variations, and topography interact. These structures strongly shape large-scale circulation and provide key pathways for energy transfer between scales (McWilliams, 1984; Vallis, 2017). When fluid encounters topographic features or other obstacles, vortex structures often form and affect the transport of momentum, heat, and tracers. Boundary-layer friction, or Ekman friction, also affects the internal velocity profile and the decay of isolated columnar vortices in rotating turbulence (Parfenyev & Vergeles, 2021). Ocean eddies range from small boundary-layer features to basin-scale eddies. They play a vital role in redistributing temperature, salinity, and important biogeochemical tracers (Wunsch, 2017; Mulligan et al., 2018). Studies by Müller & Garrett (2002), Pozorski & Wacławczyk (2020), and Caulfield (2021) show a complex link between eddies in the fluid layer and eddy diffusivity. Understanding these processes is essential to prevent irreversible pathways in geophysical fluid dynamics, such as heat and nutrient transport, and to improve the accuracy of large-scale climate models (Gregg, 2021; Liu et al., 2024).

Local vortex structures on the β-plane have been studied extensively with numerical and theoretical methods. Earlier work shows that gradients in planetary vorticity help Rossby wave packets form and evolve (Chan and William 1987). Their evolution depends strongly on the background flow, nonlinear interactions, and dissipation. Although progress has been made, analytic descriptions of local wave packets that include momentum diffusion are still scarce. Mesoscale eddies, meanwhile, mix along density surfaces by stirring tracers laterally and moving them into the water column. Ocean observations and models find that isopycnal diffusivity is highest near and above the thermocline and falls steeply with depth (Eden & Greatbatch 2009; Wolfram & Ringler 2017). The potential energy released by baroclinic instability is dissipated not by molecular viscosity but by irreversible mixing in mesoscale eddies (Garabato et al. 2011; Caulfield 2021). The interaction between Rossby wave packets and mesoscale eddies is an important question. Polvani and Plumb (1992) examined how a single coherent vortex reacts to external Rossby waves. They found a clear threshold: when the wave amplitude exceeds this value, the vortex breaks apart. Mesoscale eddies affect fluid motion through stirring. They stretch and fold gradients of properties like temperature or salinity into thin filaments. When these filaments reach a turbulent scale, eddy viscosity increases (Muller & Garrett 2002).

In geophysical fluid dynamics, unresolved turbulent motion is often represented by eddy-viscosity closures. These parameterizations describe momentum transport effectively while keeping the equations manageable. A key theoretical problem is how this effective diffusion changes the structure, propagation, and stability of localized Rossby wave packets, especially in reduced β-plane models. Fragkoulidis and Wirth (2020) showed that localized Rossby wave packets (LRWPs) exist at high latitudes. Even though the Coriolis force vanishes at the equator, observations have long documented energetic eddies there (Wyrtki & Bennett, 1963; Dickinson, 1971; Hu et al., 2022). These eddies are usually modeled with an equatorial β-field approach (Chan & Williams, 1986) and play a major role in redistributing heat, salt, and oxygen in the upper ocean. In the equatorial Eastern Indian Ocean, subsurface anticyclonic eddies (SAEs) with horizontal radii of about 250 km and cores near 100 m depth have been observed moving westward along ~4° N at ~0.18 m s^{-1} (Hu et al., 2022). Their cores are warm, salty, and oxygen-rich, have weak stratification, and can last ~100 days, strongly affecting local mixing and transport. Satellite altimetry from 1993 to 2018 identified nearly 2,800 coherent eddies in the Indo-Australian Basin, especially near major zonal currents such as the South Java Current and the Indonesian Throughflow (Ismail et al., 2021). Montgomery & Kallenbach (1997) developed the Vortex Rossby Wave (VRW) theory, which explains how Rossby wave

packets propagate radially into eddy structures and how eddy shear changes their wavenumbers. Sukoriansky et al. (2007) showed that dispersive Rossby waves on the β-plane alter the local turbulence spectrum, turning the usual eddy-viscosity coefficient into a function that depends on wave direction.

Motivated by these findings, this study builds an analytical framework using multiscale asymptotic methods and Green's function techniques to examine the perturbative dynamics of localized Rossby wave packets in weakly diffusive β-plane flows. We address two main questions: (1) how does vortex strength affect vertical eddy viscosity intensity, and vice versa? (2) how does the Rossby wavenumber relate to the eddy radius?

2. THE MODEL

2.1. Equation of Motion

We use the equation of motion in the β plane, where the generating force are the pressure gradient and gravity as (Miao *et al.,* 2022),

$$\frac{\partial u}{\partial t}+u\frac{\partial u}{\partial x}+v\frac{\partial u}{\partial y}+w\frac{\partial u}{\partial z}-\beta yv+\frac{\partial p}{\partial x}=0, \tag{1}$$

$$\frac{\partial v}{\partial t}+u\frac{\partial v}{\partial x}+v\frac{\partial v}{\partial y}+w\frac{\partial v}{\partial z}+\beta yu+\frac{\partial p}{\partial y}=0, \tag{2}$$

$$\frac{\partial w}{\partial t}+u\frac{\partial w}{\partial x}+v\frac{\partial w}{\partial y}+w\frac{\partial w}{\partial z}+g+\frac{\partial p}{\partial z}=0, \tag{3}$$

$$\frac{\partial u}{\partial x}+\frac{\partial v}{\partial y}+\frac{\partial w}{\partial z}=0, \tag{4}$$

where u,v,w are the zonal, meridional, and vertical velocity, p is the water pressure and g is the gravitational acceleration. (x,y,z) are the zonal, meridional and vertical coordinate, β is the meridional gradient of f at that fixed latitude ($\beta \sim 2.28 \times 10^{-11}$ m^{-1}s^{-1}). This partial differential equation system has solutions with both turbulent or fluctuations and a mean velocity component, where the mean is distinguished by an average over the fluctuations. To derive the mean-field balances, all fields are decomposed into mean and fluctuating component $\boldsymbol{v}=<\boldsymbol{v}>+v'$. Applying the Reynold's decomposition with white noise ($<v'>=0$), the momentum advection term can be rewritten as a momentum flux divergence which is the average of the quadratic momentum flux yields two types of contributions $\nabla.<\vec{v}\vec{v}>=<\vec{v}>$

$.\nabla < \vec{v} > + \nabla . < v'v' >$. The averaged advective flux thus has contributions both from the mean motions (the first term, the mean momentum flux) and the fluctuations (the second term, the eddy momentum flux or Reynolds stress). If the turbulence dominant in the vertical direction, the mean equation of motion become,

$$\frac{\partial U}{\partial t} + U\frac{\partial U}{\partial x} + V\frac{\partial U}{\partial y} + W\frac{\partial U}{\partial z} - \beta yV + \frac{\partial p}{\partial x} + \frac{\partial \langle u'w' \rangle}{\partial z} = 0, \qquad (5)$$

$$\frac{\partial V}{\partial t} + U\frac{\partial V}{\partial x} + V\frac{\partial V}{\partial y} + W\frac{\partial V}{\partial z} + \beta yU + \frac{\partial p}{\partial y} + \frac{\partial \langle v'w' \rangle}{\partial z} = 0, \qquad (6)$$

$$\frac{\partial W}{\partial t} + U\frac{\partial W}{\partial x} + V\frac{\partial W}{\partial y} + W\frac{\partial W}{\partial z} + g + \frac{\partial p}{\partial z} + \frac{\partial \langle w'w' \rangle}{\partial z} = 0, \qquad (7)$$

$$\frac{\partial U}{\partial x} + \frac{\partial V}{\partial y} + \frac{\partial W}{\partial z} = 0, \qquad (8)$$

here, we have use notation $< \vec{v} >= (U, V, W)$. Assuming vertical velocity small compare to horizontal, yields,

$$\frac{\partial U}{\partial t} + U\frac{\partial U}{\partial x} + V\frac{\partial U}{\partial y} - \beta yV + \frac{\partial p}{\partial x} + \frac{\partial \langle u'w' \rangle}{\partial z} = 0, \qquad (9)$$

$$\frac{\partial V}{\partial t} + U\frac{\partial V}{\partial x} + V\frac{\partial V}{\partial y} + \beta yU + \frac{\partial p}{\partial y} + \frac{\partial \langle v'w' \rangle}{\partial z} = 0, \qquad (10)$$

$$g + \frac{\partial p}{\partial z} + \frac{\partial \langle w'w' \rangle}{\partial z} = 0, \qquad (11)$$

$$\frac{\partial U}{\partial x} + \frac{\partial V}{\partial y} = 0, \qquad (12)$$

Further, we use a new second-order turbulence closure scheme that is similar to the Mellor-Yamada turbulence closure. It states that the turbulent kinetic energy can be treated prognostically, while the others are determined diagnostically. We propose to obtain these turbulent fluxes diagnostically through the following relationships (Mellor and Yamada 1982),

$$\langle u'w' \rangle = -\kappa_m \frac{\partial U}{\partial z} \quad , \quad \langle v'w' \rangle = -\kappa_m \frac{\partial V}{\partial z} \qquad (13)$$

where κ_m is the eddy-viscosity coefficient. Using a shear planetary boundary layer (<*w'w'*>=0), and stream function ($U=-\partial\psi/\partial y$, $V=\partial\psi/\partial x$), Eq.(5), Eq.(6) and Eq.(7) yields,

$$-\frac{\partial^2\psi}{\partial t\partial y}+\frac{\partial\psi}{\partial y}\frac{\partial^2\psi}{\partial x\partial y}-\frac{\partial\psi}{\partial x}\frac{\partial^2\psi}{\partial y^2}-\beta y\frac{\partial\psi}{\partial x}+\frac{\partial p}{\partial x}+\kappa_m\frac{\partial^3\psi}{\partial y\partial z^2}=0, \tag{14}$$

$$\frac{\partial^2\psi}{\partial t\partial x}-\frac{\partial\psi}{\partial y}\frac{\partial^2\psi}{\partial x^2}+\frac{\partial\psi}{\partial x}\frac{\partial^2\psi}{\partial y^2}-\beta y\frac{\partial\psi}{\partial y}+\frac{\partial p}{\partial y}-\kappa_m\frac{\partial^3\psi}{\partial x\partial z^2}=0, \tag{15}$$

Derive Eq. (14) respect to y and derive Eq. (15) respect to x, this yields,

$$\frac{\partial\nabla_H\psi}{\partial t}+J\left[\psi,\nabla_H^2\psi\right]+\beta\frac{\partial\psi}{\partial x}-\kappa_m\frac{\partial^2\nabla_H^2\psi}{\partial z^2}=0, \tag{16}$$

With the Jacobian and Laplacian are given by,

$$J\left[\psi,\nabla_H^2\psi\right]=\frac{\partial\psi}{\partial x}\frac{\partial\nabla_H^2\psi}{\partial y}-\frac{\partial\nabla_H^2\psi}{\partial x}\frac{\partial\psi}{\partial y}=0 \quad , \quad \nabla_H^2\psi=\frac{\partial^2\psi}{\partial x^2}+\frac{\partial^2\psi}{\partial y^2} \tag{17}$$

2.2. Multiple Scale Expansion Approach

This paper aim to examine the relationship between eddy characteristics (such as speed and intensity) and the eddy viscosity, which is represented by the eddy viscosity coefficient. The current framework is based on a horizontally dominant coherent vortex situated within a homogeneous layer, with a small aspect ratio (thin layer parameter) of $\varepsilon=H/L\ll1$, where H represents the vertical length scale and L the horizontal length scale. In this case, we define $x=Lx^*, y=Ly^*, z=Hz^*, \psi=UL\psi^*$, with U is a characteristic horizontal velocity scale. The nonlinear Jacobian scales as $J=\frac{U^2}{L^2}$ and the linear β-term scales as $\beta\frac{\partial\psi}{\partial x}=\beta U$, thus we have $J\Big/\beta\frac{\partial\psi}{\partial x}=\frac{U}{\beta L^2}=R_o$. This is called the Rossby number, measures the ratio between inertial (nonlinear J) effects and planetary vorticity gradient effects. Assuming $R_o = O(\varepsilon)$ implies that β-plane dynamics dominate over nonlinear advection, so that eddy evolution is primarily controlled by large-scale geostrophic balance with weak nonlinear correction. Applying non dimensional variable and ignore *, we arrive,

$$\frac{\partial\nabla_H\psi}{\partial t}+\varepsilon J\left[\psi,\nabla_H^2\psi\right]+\beta\frac{\partial\psi}{\partial x}-\kappa_m\frac{\partial^2\nabla_H^2\psi}{\partial z^2}=0, \tag{18}$$

In this weakly baroclinic, thin-layer asymptotic regime, vertical shear scale as higher-order terms relative to the leading horizontal dynamics. As a consequence, the horizontal kinetic energy of the vortex core is asymptotically larger than the energy associated with vertical

difusivity processes. Vertical eddy viscosity primarily as a higher-order correction that gradually alters the vortex amplitude and peripheral shear, rather than immediately destroying the vortex structure.

As previously mentioned, vertical speed can be disregarded in comparison to horizontal speed. Therefore, we separate the variables into horizontal and vertical functions, as outlined below,

$$\psi(x,y,z,t) = \eta(x,y,t)\phi(z) \tag{19}$$

Substituting into Eq. (18), yields,

$$\frac{\partial \nabla_H \eta}{\partial t} + \varepsilon J\left[\eta, \nabla_H^2 \eta\right] + \beta \frac{\partial \eta}{\partial x} - \nabla_H^2 \eta \frac{\kappa_m}{\phi} \frac{d^2\phi}{dz^2} = 0, \tag{20}$$

In this approach we ignore the multiplication terms between the horizontal (η) and vertical (ϕ) solutions in Jacobian (J). Thus, from the last term, we have generalized eigen value problems as follow,

$$\frac{d}{dz}\left[\kappa_m(z)\frac{d\phi_n(z)}{dz}\right] = \lambda_n \phi_n(z), \qquad \phi_n(z) = \frac{A_{\pm}}{\left(\lambda_n \kappa_m(z)\right)^{1/4}} \exp\left[\pm \int \left(\frac{\lambda_n}{\kappa_m(z)}\right)^{\frac{1}{2}} dz\right], \tag{21}$$

n = 1,2,3…, where solition is obtained using the WKB methods. The vertical eigenvalue λ_n is not prescribed independently. It emerges from the vertical diffusion operator and therefore depends explicitly on the eddy-viscosity coefficient κ_m. Consequently, variations in eddy viscosity modify the vertical eigen structure and indirectly control the horizontal evolution. Thus the horizontal equation is ,

$$\frac{\partial \nabla_H \eta}{\partial t} + \varepsilon J\left[\eta, \nabla_H^2 \eta\right] + \beta \frac{\partial \eta}{\partial x} - \lambda \nabla_H^2 \eta = 0. \tag{22}$$

We employ a multiple-scale expansion approach, allowing us to analytically solve the problem. Further, multi-scale analysis (linearized) is a technique in perturbation theory that is applicable to systems with different spatio-temporal scale characteristics. An example of a temporal scale that is very well known is an oscillator with a damping force whose damping effect is not visible on a short-term scale but is visible on a long-term scale (Holmes 2011). This approach enables us to discern dominant phenomena while acknowledging others that may not be as prominent. The linearization of the governing equations is particularly applicable within the equatorial thermocline, a layer characterized by a smooth, continuous

vertical temperature gradient. In this region, the stratification generates a robust restoring force that resists vertical displacements of water parcels. This resistance reduces the intensity of turbulence, allowing the flow to remain relatively laminar and supporting the formation of organized eddies. Consequently, the simplified linear model can capture the dominant dynamics without the computational burden of fully nonlinear simulations. However, critics argue that the linear approach may overlook subtle nonlinear interactions that can become significant during extreme events or in areas with weaker stratification. Despite this limitation, the linear framework remains a useful tool for diagnosing large-scale circulation patterns and for initializing more detailed numerical models.

Since there are fast time (vortices) and slow time (difusivity) processes, we recognize these two-time scales by introducing two-time variables as fast and slow time respectively,

$$t_0 = t, \qquad t_1 = \varepsilon t, \tag{23}$$

The derivative operator becomes,

$$\frac{\partial}{\partial t} = \frac{\partial}{\partial t_0} + \varepsilon \frac{\partial}{\partial t_1}. \tag{24}$$

Substituting Eq. (24) into Eq. (22), this yields,

$$\frac{\partial}{\partial t_0}\left(\frac{\partial^2 \eta}{\partial x^2} + \frac{\partial^2 \eta}{\partial y^2}\right) + \varepsilon \frac{\partial}{\partial t_1}\left(\frac{\partial^2 \eta}{\partial x^2} + \frac{\partial^2 \eta}{\partial y^2}\right) + \varepsilon\left[\frac{\partial \eta}{\partial x}\frac{\partial}{\partial y}\left(\frac{\partial^2 \eta}{\partial x^2} + \frac{\partial^2 \eta}{\partial y^2}\right) - \frac{\partial}{\partial x}\left(\frac{\partial^2 \eta}{\partial x^2} + \frac{\partial^2 \eta}{\partial y^2}\right)\frac{\partial \eta}{\partial y}\right]$$
$$+\beta \frac{\partial \eta}{\partial x} - \lambda\left(\frac{\partial^2 \eta}{\partial x^2} + \frac{\partial^2 \eta}{\partial y^2}\right) = 0. \qquad \text{.....(25)}$$

Thus, we expand the solution as,

$$\eta = \eta^{(0)}(x, y, t_0, t_1; \varepsilon) + \varepsilon \eta^{(1)}(x, y, t_0, t_1; \varepsilon) + \varepsilon^2 \eta^{(2)}(x, y, t_0, t_1; \varepsilon) + \ldots \tag{26}$$

Substituting Eq. (26) into Eq. (25) and we arrange order by order, yields,

- Zeroth order,

$$\left(\frac{\partial}{\partial t_0} - \lambda\right)\left(\frac{\partial^2 \eta^{(0)}}{\partial x^2} + \frac{\partial^2 \eta^{(0)}}{\partial y^2}\right) + \beta \frac{\partial \eta^{(0)}}{\partial x} = 0. \tag{27}$$

We solve the equation with the rectangular boundary condition as follow,

$$\eta^{(0)}\left(0, y \middle| x', y'\right) = \eta^{(0)}\left(a, y \middle| x', y'\right) = \eta^{(0)}\left(x, 0 \middle| x', y'\right) = \eta^{(0)}\left(x, b \middle| x', y'\right) = 0 \tag{28}$$

To describe an eddy (Gaussian eddy), suppose the solution is given by,

$$\eta^{(0)}\left(x,y,t_0\right)=\zeta^{(0)}\left(x,y\right)\varphi\left(t_0\right),\qquad \zeta^{(0)}\left(x,y\right)=e^{-\alpha\left(x^2+y^2\right)}\exp\left(-ik_x x\right). \tag{29}$$

Substituting into Eq. (27) yields (see Appendix A),

$$\eta^{(0)}\left(x,y,t_0\right)=e^{-\alpha\left(x^2+y^2\right)}\exp\left(-ik_x x\right)\exp\left[\left(\lambda+i\frac{\beta k}{\left(k^2-4\alpha\right)}\right)t_0\right]. \tag{30}$$

- First order,

$$\Omega\eta^{(1)}=-\frac{\partial}{\partial t_1}\left(\frac{\partial^2\eta^{(0)}}{\partial x^2}+\frac{\partial^2\eta^{(0)}}{\partial y^2}\right)-\left[\frac{\partial\eta^{(0)}}{\partial x}\frac{\partial}{\partial y}\left(\frac{\partial^2\eta^{(0)}}{\partial x^2}+\frac{\partial^2\eta^{(0)}}{\partial y^2}\right)-\frac{\partial}{\partial x}\left(\frac{\partial^2\eta^{(0)}}{\partial x^2}+\frac{\partial^2\eta^{(0)}}{\partial y^2}\right)\frac{\partial\eta^{(0)}}{\partial y}\right].$$

…… (31)

where

$$\Omega=\frac{\partial}{\partial t_0}\left(\frac{\partial^2}{\partial x^2}+\frac{\partial^2}{\partial y^2}\right)+\beta\frac{\partial}{\partial x}-\lambda\left(\frac{\partial^2}{\partial x^2}+\frac{\partial^2}{\partial y^2}\right) \tag{32}$$

Suppose the solution is given by,

$$\eta^{(1)}\left(x,y,t_0,t_1\right)=e^{-i\omega_0 t_0}e^{-i\omega_1 t_1}\zeta^{(1)}\left(x,y\right),\qquad \omega_0=\left(\lambda+i\frac{\beta k}{\left(k^2-4\alpha\right)}\right). \tag{33}$$

Eq. (31) yields,

$$\left[\Omega\right]\zeta^{(1)}=i\omega_0\left(\frac{\partial^2\zeta^{(0)}}{\partial x^2}+\frac{\partial^2\zeta^{(0)}}{\partial y^2}\right)-\left[\frac{\partial\zeta^{(0)}}{\partial x}\frac{\partial}{\partial y}\left(\frac{\partial^2\zeta^{(0)}}{\partial x^2}+\frac{\partial^2\zeta^{(0)}}{\partial y^2}\right)-\frac{\partial}{\partial x}\left(\frac{\partial^2\zeta^{(0)}}{\partial x^2}+\frac{\partial^2\zeta^{(0)}}{\partial y^2}\right)\frac{\partial\zeta^{(0)}}{\partial y}\right],$$

……..(34)

where

$$\left[\Omega\right]=\left(\frac{\partial^2}{\partial x^2}+\frac{\partial^2}{\partial y^2}\right)-\frac{\beta}{\left[\lambda+i\omega_0\right]}\frac{\partial}{\partial x}. \tag{35}$$

The solution is given in term of Green function as follow,

$$\zeta^{(1)}\left(x,y\right)=\int_0^x\int_0^y G\left(\chi|\chi'\right)\left(i\omega_0\left(\frac{\partial^2\zeta^{(0)}}{\partial x'^2}+\frac{\partial^2\zeta^{(0)}}{\partial y'^2}\right)-\left[\begin{array}{l}\dfrac{\partial\zeta^{(0)}}{\partial x'}\dfrac{\partial}{\partial y'}\left(\dfrac{\partial^2\zeta^{(0)}}{\partial x'^2}+\dfrac{\partial^2\zeta^{(0)}}{\partial y'^2}\right)\\ -\dfrac{\partial}{\partial x'}\left(\dfrac{\partial^2\zeta^{(0)}}{\partial x'^2}+\dfrac{\partial^2\zeta^{(0)}}{\partial y'^2}\right)\dfrac{\partial\zeta^{(0)}}{\partial y'}\end{array}\right]\right)d\chi' \tag{36}$$

.

where $\chi=x,y$ and $\chi'=x',y'$ and the Green function satisfy,

$$\left(\frac{\partial^2 G(\chi|\chi')}{\partial x^2}+\frac{\partial^2 G(\chi|\chi')}{\partial y^2}\right)-\frac{\beta}{[\lambda+i\omega_0]}\frac{\partial G(\chi|\chi')}{\partial x}=-4\pi\delta(x-x')\delta(y-y'). \quad (37)$$

The Green's function is given by (see Appendix-B for detail derivation),

$$G(x,y|x',y')=-\frac{16}{ab}\sum_{m=0}^{\infty}\sum_{n=0}^{\infty}\frac{\sin^2\left(\frac{m\pi x}{a}\right)\sin\left(\frac{n\pi y}{b}\right)}{\left[C\sin\left(\frac{m\pi x}{a}\right)+D\cos\left(\frac{m\pi x}{a}\right)\right]}\sin\left(\frac{m\pi x'}{a}\right)\sin\left(\frac{n\pi y'}{b}\right),$$

……(38)

where

$$C=\left[2\Gamma^2-\left(\frac{m\pi}{a}\right)^2-\left(\frac{n\pi}{b}\right)^2\right],\quad D=\left[2\Gamma\frac{mn}{a}+\Gamma\right],\quad \Gamma=-\frac{\beta}{[\lambda+i\omega_0]}. \quad (39)$$

- Second order,

$$\begin{aligned}[\Omega]\eta^{(2)}=&\frac{\partial\eta^{(0)}}{\partial y}\left(\frac{\partial^3\eta^{(1)}}{\partial x^3}+\frac{\partial^3\eta^{(1)}}{\partial x\partial y^2}\right)+\frac{\partial\eta^{(1)}}{\partial y}\left(\frac{\partial^3\eta^{(0)}}{\partial x^3}+\frac{\partial^3\eta^{(0)}}{\partial x\partial y^2}\right)-\frac{\partial}{\partial t_1}\left(\frac{\partial^2\eta^{(1)}}{\partial x^2}+\frac{\partial^2\eta^{(1)}}{\partial y^2}\right)\\&-\frac{\partial\eta^{(0)}}{\partial x}\left(\frac{\partial^3\eta^{(1)}}{\partial y\partial x^2}+\frac{\partial^3\eta^{(1)}}{\partial y^3}\right)+\frac{\partial\eta^{(1)}}{\partial x}\left(\frac{\partial^3\eta^{(0)}}{\partial y\partial x^2}+\frac{\partial^3\eta^{(0)}}{\partial y^3}\right).\end{aligned} \quad (40)$$

With the same mathematical structure as Eq. (34), the solution is expressed as follows,

$$\zeta^{(2)}(x,y)=\int_0^{t_0}\int_0^{x}\int_0^{y}G(\chi|\chi')\left(\begin{array}{l}\frac{\partial\zeta^{(0)}}{\partial y}\left(\frac{\partial^3\zeta^{(1)}}{\partial x^3}+\frac{\partial^3\zeta^{(1)}}{\partial x\partial y^2}\right)+\frac{\partial\zeta^{(1)}}{\partial y}\left(\frac{\partial^3\zeta^{(0)}}{\partial x^3}+\frac{\partial^3\zeta^{(0)}}{\partial x\partial y^2}\right)\\ i\omega_0\left(\frac{\partial^2\zeta^{(1)}}{\partial x^2}+\frac{\partial^2\zeta^{(1)}}{\partial y^2}\right)-\frac{\partial\zeta^{(0)}}{\partial x}\left(\frac{\partial^3\zeta^{(1)}}{\partial y\partial x^2}+\frac{\partial^3\zeta^{(1)}}{\partial y^3}\right)\\ +\frac{\partial\zeta^{(1)}}{\partial x}\left(\frac{\partial^3\zeta^{(0)}}{\partial y\partial x^2}+\frac{\partial^3\zeta^{(0)}}{\partial y^3}\right)\end{array}\right)d\chi' \quad (41)$$

with

$$\eta^{(2)}(x,y,t_0,t_1)=e^{-i\omega_1 t_1}\zeta^{(2)}(x,y), \quad (42)$$

The structure of the equation has the same pattern for subsequent orders, so we show only consider up to the second order.

3. RESULTS AND DISCUSSIONS

3.1. Zeroth-order Gaussian vortex structure

A Gaussian eddy profile was adopted as the zero-order solution to represent the leading-order state, because its shape mirrors the structure of coherent vortices found in equatorial waters (Carton, 2001). The Gaussian velocity field, which decays smoothly with distance from the center, allows the flow to reach a stable leading-order equilibrium within the quasi-geostrophic approximation before any instability develops. Once the flow is in this state, the barotropic shear instability that arises from the velocity gradient becomes the dominant mechanism for converting organized kinetic energy into smaller-scale motions, thereby increasing dissipation. At the same time, the instability facilitates vertical momentum transport, redistributing momentum from the upper layers to the lower layers in the equatorial region. Therefore, while the barotropic shear instability plays a primary role in this context, it should be considered alongside other potential drivers when evaluating the full dynamics of the equatorial system. Thus we write the Eq.(30) as,

$$\eta^{(0)}\left(x,y,t_0\right)=\frac{V_0R}{2}e^{-\frac{\left((x-x_c)^2+(y-y_c)^2\right)}{R^2}}\exp\left(-ik_x x\right)\exp\left[\left(\lambda+i\frac{\beta k}{\left(k^2-\frac{4}{R^2}\right)}\right)t_0\right]. \tag{43}$$

where R is eddy length scale, and the eigen value is given by $\lambda_n = -\kappa_m(n\pi/H)^2$. On the other hands, to assess how eigen value λ_n and Rossby factor β affect transport and vertical turbulent momentum diffusion (hereafter simply called eddy viscosity), this simulation employs a Lagrangian passive tracer method. Tracer particles are released in the flow field to chart the deformation of the water mass caused by the stream function ($dx_p/dt = (\partial\eta/\partial y)_{(xp,yp,t)}$) and $dy_p/dt = -(\partial\eta/\partial x)_{(xp,yp,t)}$). This is depicted in Figure 1. Fig. 1 shows the zeroth-order solution. It is a localized Rossby wave packet that is modulated by a Gaussian vortex envelope. The envelope reaches its maximum at r =0, so the streamfunction gradients are strongest near the vortex core. Tracer particles released close to the center therefore follow almost closed paths and stay trapped inside the coherent core. These tracers are used to illustrate the rotation of the Gaussian eddy. Far from the core ($r >> R$), the Gaussian envelope tend to weakens, so the vortex circulation has less restoring force. Peripheral tracers are then more strongly deformed and their paths become more spread out. This shows the difference between the tightly trapped region near the vortex center and the outer region where particle dispersion is large.

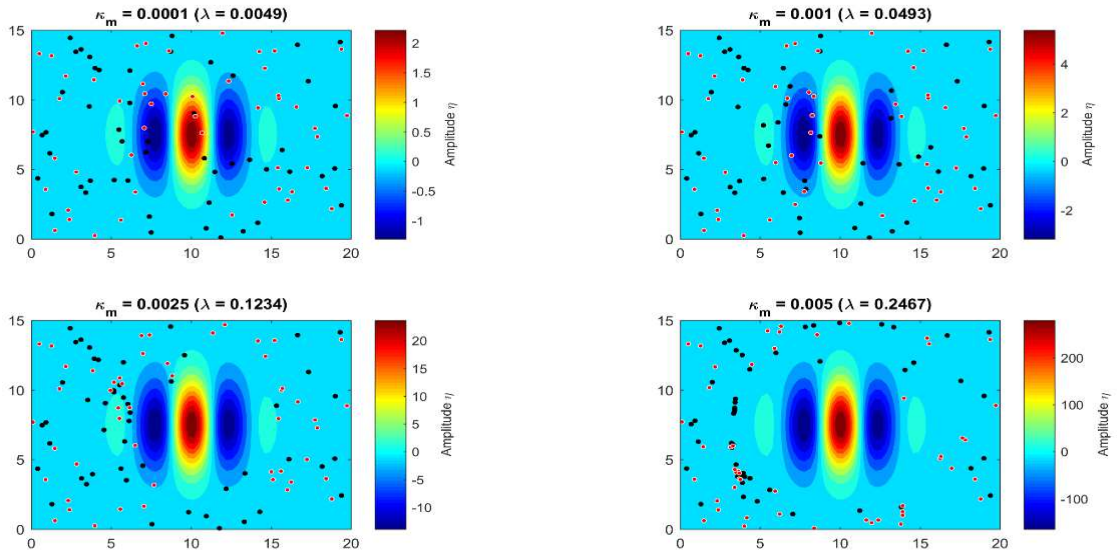


Figure 1. Temporal evolution of Lagrangian particles in a Gaussian eddy on the equatorial β-plane at t 1 to 20 s. Arrows show current velocity (u, v). Black dots are core-trapped particles; green dots are peripheral particles. We use a logarithmic normalization for visualization and $n = 1$.

The variation in the λ_n value of the horizontal stream function (η) reflects the eigenvalue solution (λ_n) obtained from the Eq.(21) for a range of eddy viscosity coefficients κ_m. This dependence arises because κ_m directly influences structure of eddy, which in turn alter the vertical structure of the eigen functions that determine λ_n. Consequently, changes in κ_m modify the dispersion pattern of the horizontal flow, revealing how sensitive eigen function dynamics are to vertical eddy viscosity processes. The sensitivity indicates that even modest adjustments in κ_m can lead to measurable shifts in the horizontal current structure, potentially affecting transport and eddy viscosity rates in the studied system. Ultimately, understanding the link between κ_m and λ_n provides a valuable diagnostic tool for assessing the role of vertical diffusivity in shaping large-scale horizontal currents. The other hands, in a stratified flow, however, such eddies tend to flatten the isopycnals (density contours). The simulations confirm that the Gaussian model contains a vorticity core, may mirroring the behaviour of Tropical Instability Eddies (TIEs) at the equator, which maintain coherence for several days (Lyman et al., 2005; Shi et al., 2021). Meanwhile, the dots are in the outer or peripheral zone, where these particles exhibit broader movement patterns and are susceptible to deformation.

3.2. Sensitivity of eddy viscosity to eddy formation

To quantitatively assess how eddy viscosity strength influences eddy formation, we plot the eddy coefficient against the mean dispersion index, which quantifies the radial distance of a tracer from the eddy center. The index was defined $\delta =$

$\frac{1}{N}\Sigma\sqrt{\left(x_{pi}(t)-x_c\right)^2+\left(y_{pi}(t)-y_c\right)^2}$ measures the radial distance of tracer particles from the center of the eddy. *N* is the particle number and $(x_{p,i},y_{p,i})$ is the particle position respect to the center of eddy (x_c,y_c) (see LaCasce 2008). This is depicted in Figure 2. The figure reveals that as the eddy viscosity coefficient rises, the dispersion index also increases, but the trend is not linear; instead, it follows an exponential pattern. This exponential growth suggests that stronger stirring causes the eddy to expand more rapidly, thereby enlarging its effective radius. Consequently, a wider eddy can be interpreted as a marker of intense eddy viscosity activity. However, some researchers argue that other factors such as background flow shear or buoyancy effects may also contribute to eddy size, implying that eddy viscosity strength alone may not fully explain the observed expansion (Smith 2007, Chelton *et al.,* 2011).

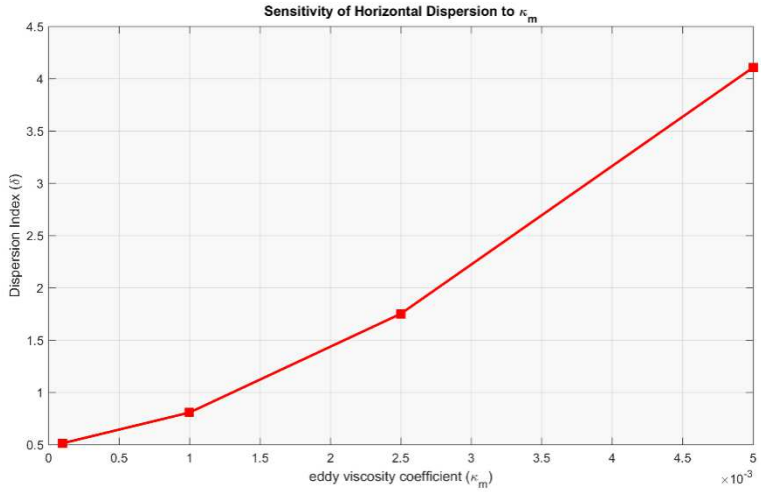


Figure 2. Sensitivity of the horizontal dispersion index (δ) to changes in the vertical eddy viscosity coefficient (κ_m). The nonlinear, exponential trend shows that higher vertical turbulent diffusion accelerates the loss of the vortex core's resilience.

3.3 Radius effect of Rossby-wave propagation

The Gaussian eddy has simple solution in the form of $\eta^{(0)}=Aexp\left(-\frac{r^2}{R^2}\right)cos(kx-\omega t)$, *R* is the eddy radius, and when $r^2=(x-x_c)^2+(y-y_c)^2$, substituting into the Eq. (27) and approximation $r << R$, we arrive the dispersion relations $\omega=-\beta k/\left(k^2+\frac{4}{R^2}\right)$. This is called the dispersion relation for vortex Gaussian Rossby wave packet. In this case the group velocity is given by $c_g=\beta\left(k^2-\frac{4}{R^2}\right)/\left(k^2+\frac{4}{R^2}\right)^2$. It is note that the conventional Rossby wave dispersion relation is $\omega=\beta k/(k^2+l^2)$ represent Westward wave propagation.

Having established the particle trajectory trapping properties of the zeroth-order Gaussian vortex (Figure 1), we now examine its wave aspect of the same solution. The

zeroth-order streamfunction is a Rossby wave modulated by a Gaussian envelope, forming a Localized Rossby Wave Packet (LRWP) where the vortex acts as the coherent carrier. Figure 3 shows the packet's propagation on the β-plane, tracking the envelope rather than tracer particles. The simulation confirms that the zeroth-order solution behaves as a coherent vortex while supporting Rossby-wave propagation, in line with Montgomery & Kallenbach (1997). Thus, the Gaussian vortex confines and transports Rossby-wave energy as a localized packet as shown in Figure 3. The LRWP's propagation is determined by a radius-dependent dispersion relation, while the vertical eddy-viscosity coefficient controls the growth of the perturbation through the eigenvalue λ. The term $exp(\lambda t)$ shows how energy moves from the main vortex to the surrounding perturbation field. Figure 3 also shows that the eddy coefficient only determines the magnitude of the wave packet amplitude but does not change the shape of the wave packet, while the wave number significantly determines the pattern, speed and amplitude of the wave packet.

Fragkoulidis and Wirth (2020) found that localized Rossby wave packets can exist at higher latitudes, where the wave energy stays confined while the phase moves inside the envelope. Our results suggest that similar packets can also appear in equatorial β-plane flows. Unlike a non-rotating fluid, where an isolated vortex would simply decay, the planetary-vorticity gradient allows continuous emission and organization of Rossby-wave disturbances. The sensitivity of this process to vertical mixing is shown by the dependence of the eigenvalues λ_n on the eddy-viscosity coefficient κ_m. Larger κ_m values increase the perturbation amplitude, weaken vortex confinement, and promote fluid exchange between the vortex core and its surroundings. These findings agree with observations of long-lived subsurface eddies in the eastern equatorial Indian Ocean reported by Hu et al. (2022). They described warm, saline, and oxygen-rich anticyclonic eddies with horizontal radii over 250 km that played a key role in transporting water masses and tracers. The present analytical framework offers a dynamical explanation for how coherent equatorial eddies can release energy into surrounding Rossby-wave disturbances and help redistribute heat, salinity, oxygen, and water mass through wave propagation and turbulent diffusion.

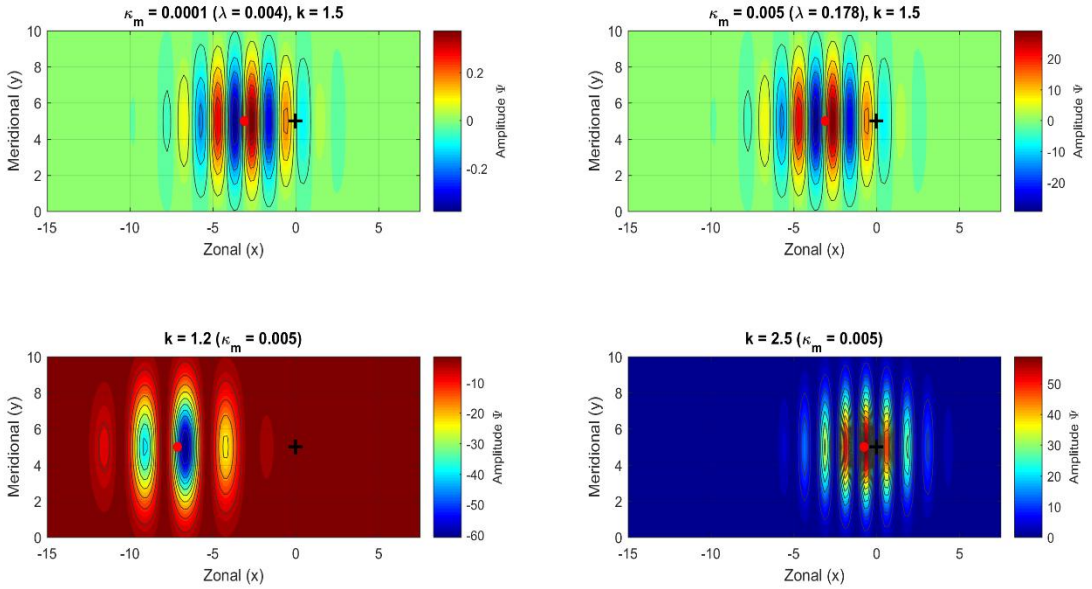


Figure 3. Spatial structure and propagation of the LRWP streamfunction at t = 25 under two extreme vertical diffusion regimes: weakly dissipative ($\kappa_m = 0.0001$, $\lambda = 0.0036$) and strongly diffusive ($\kappa_m = 0.005$, $\lambda = 0.1777$). The black cross marks the initial wave center, and the red circle shows the downstream position of the wave envelope, indicating eastward phase propagation.

The β effect stretches the vortex westward but does not shift its center, as shown by the dispersion far from the eddy center in Figure 1. When the vortex shape remains constant, its northward drift is governed by the background wind speed (Chen & Williams 1987). A 22-day, 3600-km equatorial Rossby wave packet in the lower troposphere of the Northwest Pacific propagated westward at 1.9 m s^{-1}, had near-zero group speed, and existed over an eastward background wind. The packet was linked to at least 8 of 13 tropical cyclones that formed during the period. Rossby wave packets can precede flow anomalies such as blocking or intense cyclones, potentially causing severe weather at high latitudes (Ghinassi et al. 2018; Kedzierski et al. 2020). Our findings also confirm wave localization, with wavelength tied to the vortex radius scale.

3.4 First-order Green-function correction

After establishing that the eddy can stably trap water masses at the lowest order of stability (zeroth-order), the next logical step is to examine the mechanisms by which minor perturbations at the eddy's periphery can compromise this equilibrium. Small-scale disturbances such as wind-driven shear, buoyancy anomalies, or topographic interactions can introduce kinetic energy into the boundary layer, thereby weakening the coherent rotational structure that maintains the trapped water (Dewar 2002). This destabilization initiates a cascade of vertical motions, as the eddy's internal stratification is disrupted and parcels of water are

forced to exchange with surrounding layers. The resulting vertical eddy viscosity enhances nutrient transport and heat redistribution, which can have significant ecological and climatic implications (Eden and Dietze 2009). However, some studies argue that the eddy's inherent resilience may absorb these perturbations without leading to substantial eddy viscosity, suggesting that additional thresholds of disturbance magnitude or duration are required. Moreover, the role of ambient turbulence and background currents may either amplify or dampen the eddy viscosity response, depending on the specific oceanographic context. Consequently, while small disturbances are a plausible trigger for vertical eddy viscosity, the extent of their impact remains contingent upon a complex interplay of dynamical and environmental factors.

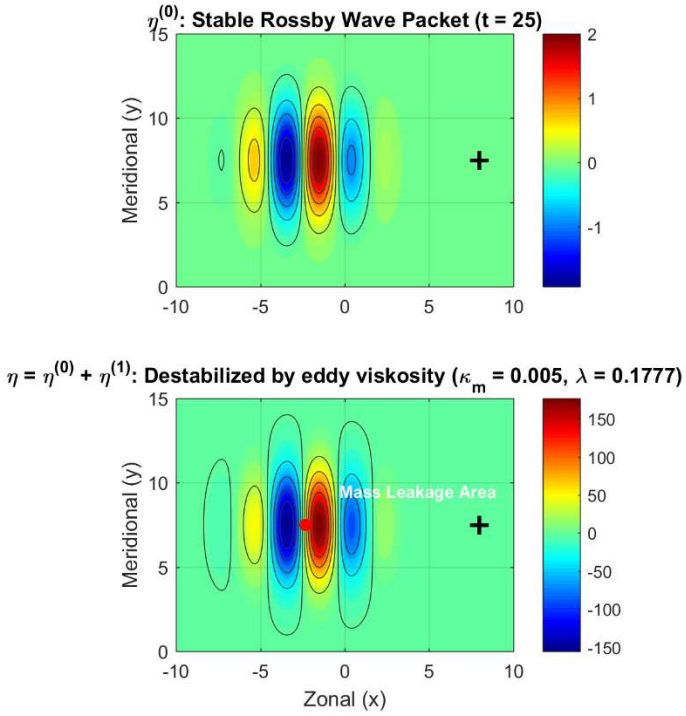


Figure 4. Propagation of Localized Rossby Wave Packet with first-order effect.

The effect of first-order is depicted in Figure 4. It displays a simulation of the first-order effect, revealing extra vorticity structures that develop around the primary wave packet. The disturbance not only reduces the packet's amplitude but also generates secondary vortices or additional wave-envelope features along the zonal (x-axis) side. Mathematically, this arises from the Fourier-series sum in the Green's function, which represents the system's response to nonlinear (Jacobian) perturbations. The extra structure demonstrates that peripheral disturbances begin to destabilise the otherwise stable zeroth-order equilibrium. Ripples forming beyond the main core indicate that the energy once confined is now dispersing, a

process that may trigger a chain reaction; in other words, small perturbations can break the eddy's coherent state and scatter the wave packet sideways such as energy cascade (Müller & Garrett 2002).

Previous studies have shown that external disturbances such as topographic variations, atmospheric flow fluctuations, and dissipative forcing significantly affect the stability and subsequent evolution of Rossby wave packets (Zhang et al., 2019). These disturbances alter the wave propagation characteristics, causing changes in their amplitude, phase velocity, and spatial structure. This paper further details how Rossby wave structures are modified when encountering a non-uniform environment, noting that such interactions can generate additional wave modes and modify existing ones. As a result, equatorial Rossby wave packets can interact and combine to form more complex structures, including TIEs, which play a key role in redistributing heat across the tropics (Lyman et al., 2005). These results reiterate that the interplay between external disturbances and Rossby wave dynamics is crucial for understanding large-scale tropical variability and its impact on global climate patterns (Pinault 2026).

4. CONCLUSIONS

This study introduces an analytical framework to examine localized Rossby wave packets in weakly diffusive β-plane flows. We use multiscale asymptotic expansion and Green-function methods. Starting from the incompressible momentum equations with a Mellor–Yamada eddy-viscosity closure, we derive a simplified stream function model. In this model, vertical turbulent diffusion influences horizontal motion through a vertical eigenvalue problem. The leading-order solution is a localized Gaussian vortex that remains coherent and traps fluid parcels inside its core. The vertical eigenvalue arises naturally from the diffusion operator and is the main way the eddy-viscosity coefficient affects horizontal flow. Numerical tracer experiments show that higher eddy viscosity increases particle dispersion and weakens vortex confinement. A key result is a radius-dependent Rossby-wave dispersion relation. Unlike the classical relation, this formulation predicts a critical radius that separates eastward from westward propagation. Thus, the vortex radius controls the direction and characteristics of the localized Rossby-wave packet. The Green-function solution reveals that first-order perturbations generate secondary vorticity structures and distort the wave envelope around the primary packet. These higher-order corrections redistribute energy laterally and gradually break down coherent vortex structures when diffusion is weak and nonlinear perturbations are present. Overall, the framework analytically links vertical turbulent diffusion, vortex

eigenstructure, and localized Rossby-wave dynamics. The results provide a theoretical basis for future investigations of coherent structures, mesoscale eddies, and wave-vortex interactions in geophysical fluid dynamics.

ACKNOWLEDGEMENT

This research was funded by DIPA BRIN for fiscal year 2026.

Declarations Conflict of interest

The authors declare no conflict of interest.

Funding

The authors received no financial support for the research, authorship, and/or publication of this article.

Trial Registration:

Not Applicable.

REFERENCES

[1]. Carton, X. J. (2001). Hydrodynamical modeling of oceanic vortices. *Surveys Geophys*., 22, 179–. 263.

[2]. Caulfield,C.P., (2021). Layering, Instabilities, and Mixing in Turbulent Stratiefied Flow, *Annual Review of Fluid Mechanics*, 53, 113-145.

[3]. han, J. C. L., and R. T. Williams, (1987). Analytical and Numerical Studies of the Beta-Effect in Tropical Cyclone Motion. Part I: Zero Mean Flow. *J. Atmos. Sci*., 44, 1257–1265.

[4]. Chan, J.C.L., and Williams, R.T., (1986). Analytical and numerical studies of the beta-effect in tropical cyclone motion. Part I: zero mean flow, *J. Atmo. Sc*i, 44,9, 1257-1266.

[5]. Chelton, D.B., Schlax, M.G., Samelson,R.M., (2011). Global observations of nonlinear mesoscale eddies., *Prog. Oceanogr.*, 91 (2), 167-216.

[6]. Dewar, W. K., (2002). Baroclinic Eddy Interaction with Isolated Topography. *J. Phys. Oceanogr*., 32, 2789–2805, https://doi.org/10.1175/1520-

[7]. Dickinson, R.E., (1971). Cross-equatorial eddy momentum fluxes as evidence of tropical planetary wave sources, *Quarterly J. Royal Met. Soc*, 97, 414, 554-558.

[8]. Eden,C and Dietze,H., (2009). Effects of mesoscale eddy/wind interactions on biological new production and eddy kinetic energy., *J. Geophys. Res*., 114 (C5), C05023-C05036. https://doi.org/10.1029/2008JC005129.

[9]. Eden,C., and Greatbatch, R.J., (2009). A diagnosis of isopycnal mixing by mesoscale eddies, *Ocean Modelin*g, 27,1, 98-106.

[10]. Fragkoulidis,G and Wirth,V., (2020). Local Rossby Wave Packet Amplitude, Phase Speed, and Group Velocity: Seasonal Variability and Their Role in Temperature Extremes., *J. Climate*., 33, 8767-8261.

[11]. Garabato, N. A. C., R. Ferrari, and K. L. Polzin., (2011). Eddy stirring in the Southern Ocean, *J. Geophys. Res.*, 116, C09019, doi:10.1029/2010JC006818.

[12]. Ghinassi, P., M. Baumgart, F. Teubler, M. Riemer, and V. Wirth, (2020). A Budget Equation for the Amplitude of Rossby Wave Packets Based on Finite-Amplitude Local Wave Activity. *J. Atmos. Sci*., 77, 277–296, https://doi.org/10.1175/JAS-D-19-0149.1

[13]. Gregg, M.C., (2021)., *Ocean Mixing* , Cambridge University Press, 409 pp.

[14]. Holmes, M.H.(2011). *Introduction to perturbation methods*, Springer-Verlag, Berlin, 451 pp.

[15]. Hu,Z., Ma, X., Peng,Y., Tian,D., Meng,Q., Zeng,D., Liu, Z., Zhou, B., Li, H., Zhou, F., (2022). A Large Subsurface Anticyclonic Eddy in the Eastern Equatorial Indian Ocean, *J. Geophys. Res*, 127, 3, 22021JCO18130.

[16]. Ismail, M. F.A ., Ribbe, J., Arifin,T., Taofiqurohman, A., & Anggoro, D. (2021). A census of eddies in the tropical eastern boundary of the Indian Ocean. *J. Geophys. Res: Oceans*, *126*, e2021JC017204. https:// doi.org/10.1029/2021JC017204.

[17]. Kedzierski,P., Matthes,R., Bumke, K., (2020). New insights into Rossby wave packet properties in the extratropical UTLS using GNSS radio occultations, J. Atmospheric Chemistry and Physics, 20, 19, 11569--11592. DOI = 10.5194/acp-20-11569-2020.

[18]. LaCasce, J.H., (2008). Review of Lagrangian Analysis and Prediction of Coastal and Ocean Dynamics, edited by A. Griffa, A.D. Kirwan Jr., A.J. Mariano, T. Özgökmen, and H.T. Rossby. *Oceanogr.* 21 (2), 78–81, https://doi.org/10.5670/oceanog.2008.62.

[19]. Liu, Y., Li, Y., Xue, J., Dai, P., Gu, Y., Lu, H., Yang, Q., (2024). Study on the unique separation effect of emulsion in the stirring-induced turbulent flow field, *Journal of Cleaner Production*, 478, 143864, https://doi.org/10.1016/j.jclepro.2024.143864.

[20]. Lyman, J. M., D. B. Chelton, R. A. deSzoeke, and R. M. Samelson, (2005). Tropical Instability Waves as a Resonance between Equatorial Rossby Waves. *J. Phys. Oceanogr*., 35, 232–254, https://doi.org/10.1175/JPO-2668.1.

[21]. McWilliams, J. C., (1984). The emergence of isolated coherent vortices in turbulent Macrodynamics. *J. Fluid Mech*, 146, 21-43.

[22]. Mellor, G. L. and Yamada, T., (1982). Development of a turbulence closure model for geophysical fluid problems. *Rev. Geophys. Space Phys.*, 20, 851-875.

[23]. Miao, F., Fečkan, M. and Wang, J. (2022). Constant vorticity water flows in the modified equatorial β-plane approximation. *Monatsh Math* **197**, 517–527. https://doi.org/10.1007/s00605-021-01571-3.

[24]. Montgomery, M. T., & Kallenbach, R. J., (1997). A theory for vortex Rossby-waves and its application to spiral bands and intensity changes in hurricanes, Q. J. R. Meteorol. Soc., 123 (538), 435-465.

[25]. Müller, P., & Garrett, C. (2002). From Stirring to Mixing in a Stratified Ocean. *Oceanogr*, 15(3), 12-19.

[26]. Mulligan, S., De Cesare, G., Casserly, J. *et al.,* (2018). Understanding turbulent free-surface vortex flows using a Taylor-Couette flow analogy. *Sci Rep* **8**, 824. https://doi.org/10.1038/s41598-017-16950-w.

[27]. Parfenye,V.M and S.S Vergeles., (2021). Influence of Ekman friction on the velocity profile of a coherent vortex in a three-dimensional rotating turbulent flow., Physics of Fluids 33, 115128. https://doi.org/10.1063/5.0072734

[28]. Pinault, J.L., (2026). Resonant Forcing of Oceanic and Atmospheric Rossby Waves in (Sub) Harmonic Modes: Climate Impacts., *Atmosphere*, 17, 127. https://doi.org/10.3390/atmos17020127

[29]. Polvani, L. M., and R. A. Plumb., (1992). Rossby Wave Breaking, Microbreaking, Filamentation, and Secondary Vortex Formation: The Dynamics of a Perturbed Vortex. *J. Atmos. Sci*., 49, 462–476, https://doi.org/10.1175/1520-0469(1992)049<0462:RWBMFA>2.0.CO;2.

[30]. Pozorski, J.; Wacławczyk, M. (2020). Mixing in Turbulent Flows: An Overview of Physics and Modelling. *Processes* , *8*, 1379. https://doi.org/10.3390/pr8111379.

[31]. Shi, W., Lin, H., Deng, Q., & Hu, J. (2024). Asymmetry of submesoscale instabilities in anticyclonic and cyclonic eddies. *Geophy. Res. Let*, 51, e2023GL106853. https://doi.org/10.1029/2023GL106853.

[32]. Smith, K. S., 2007. The geography of linear baroclinic instability in Earth's oceans. J. Mar. Res. 65, (5).

[33]. Sukoriansky, S., Galperin, B., and Staroselsky, I. (2007). Geophysical flows with anisotropic turbulence and dispersive waves: Flows with a β-effect. *Ocean Dynam*, 57, 203–214.

[34]. Vallis, G. K. (2017). *Atmospheric and Oceanic Fluid Dynamics: Fundamentals and Large-scale Circulation,* 2nd edition, Cambridge University Press, 960pp.

[35]. Wolfram, P.J., Ringler, T.D., (2017). Quantifying residual, eddy, and mean flow effects on mixing in an idelaized circumpolar currents, *J. Phys. Oceanorg*, 47, 1897-1911,.

[36]. Wunsch, C., (2007). Ocean Mixing. Oxford Research Encyclopedia of Climate Science. Retrieved 1 Feb. 2024, from https://oxfordre.com/climatescience/view/ 10.1093/ acrefore/ 9780190228620.001.0001/ acrefore-9780190228620-e.

[37]. Wyrki,K., and Bennett, E.B., (1963). Vertical eddy viscosity in the Pacific equatorial undercurrents, *Deep-sea Res*, 10, 449-455.

[38]. Zhang, R., Yang, L., Liu, Q., Yin, X, (2019). Dynamics of nonlinear Rossby waves in zonally varying flow with spatial-temporal varying topography, *Appl. Math. Comput*., 346, 666-679. https://doi.org/10.1016/j.amc.2018.10.084.

Appendix A: Gaussian-like solution of Eq.(30)

First we calculate,

$$\frac{\partial \eta^{(0)}}{\partial x} = \left(-\alpha x - ik\right) e^{-\alpha\left(x^2+y^2\right)} \exp\left(-ikx\right) \varphi\left(t_0\right), \tag{A1}$$

$$\frac{\partial^2 \eta^{(0)}}{\partial x^2} = \left[4\alpha^2 x^2 - 2\alpha + k^2 - i4\alpha k\right] e^{-\alpha\left(x^2+y^2\right)} \exp\left(-ikx\right) \varphi\left(t_0\right), \tag{A2}$$

$$\frac{\partial^2 \eta^{(0)}}{\partial y^2} = \left[4\alpha^2 y^2 - 2\alpha\right] e^{-\alpha\left(x^2+y^2\right)} \exp(-ikx) \varphi\left(t_0\right), \tag{A3}$$

Assuming $\alpha x = \alpha y \sim 0$, $\alpha k = 0$, substituting into Eq. (27), we arrive,

$$\left(\frac{\partial \varphi\left(t_0\right)}{\partial t_0} - \lambda \varphi\left(t_0\right)\right)\left(k^2 - 4\alpha\right) - i\beta k \varphi\left(t_0\right) = 0. \tag{A4}$$

We write

$$\frac{\partial \varphi\left(t_0\right)}{\partial t_0} - \left[\lambda + i\frac{\beta k}{\left(k^2 - 4\alpha\right)}\right] \varphi\left(t_0\right) = 0. \tag{A5}$$

The solution is given by,

$$\varphi\left(t_0\right) \sim \exp\left[\left(\lambda + i\frac{\beta k}{\left(k^2 - 4\alpha\right)}\right) t_0\right]. \tag{A6}$$

We have complete solution.

Appendix B: Determine of the Green Function

$$\frac{\partial^2 G(x,y|x',y')}{\partial x^2}+\frac{\partial^2 G(x,y|x',y')}{\partial y^2}+\Gamma\frac{\partial G(x,y|x',y')}{\partial x}=-4\pi\delta(x-x')\delta(y-y'), \quad \text{(A1)}$$

with $\Gamma=-\beta/[\lambda+i\omega_0]$. Subject to the boundary condition which states the solution is confined within a box,

$$G(0,y|x',y')=G(a,y|x',y')=G(x,0|x',y')=G(x,b|x',y')=0. \quad \text{(A2)}$$

We find the Green function as follow, first express the Green function and Dirac function as the double of Fourier series,

$$\begin{aligned} G(x,y|x',y') &= \sum_{m=0}^{\infty}\sum_{n=0}^{\infty} A_{mn}e^{\Gamma x}\sin\left(\frac{m\pi x}{a}\right)\sin\left(\frac{n\pi y}{b}\right), \\ \delta(x-x')\delta(y-y') &= \sum_{m=0}^{\infty}\sum_{n=0}^{\infty} B_{mn}\sin\left(\frac{m\pi x}{a}\right)\sin\left(\frac{n\pi y}{b}\right). \end{aligned} \quad \text{(A3)}$$

Thus, we determine B_{mn} using orthogonality function,

$$\begin{aligned} &\int_{-\infty}^{\infty}\int_{-\infty}^{\infty}\delta(x-x')\delta(z-z')\sin\left(\frac{m\pi x}{a}\right)\sin\left(\frac{n\pi y}{b}\right)dxdy = \\ &\int_{-\infty}^{\infty}\int_{-\infty}^{\infty}\sum_{m=0}^{\infty}\sum_{n=0}^{\infty}B_{mn}\sin\left(\frac{m\pi x}{a}\right)\sin\left(\frac{n\pi y}{b}\right)\sin\left(\frac{m\pi x}{a}\right)\sin\left(\frac{n\pi y}{b}\right)dxdy=0. \end{aligned} \quad \text{(A4)}$$

Using the trigonometric integral

$$\int_0^a \sin\left(\frac{m\pi x}{a}\right)\sin\left(\frac{m\pi x}{a}\right)dx=\frac{a}{2} \quad , \quad \int_0^b \sin\left(\frac{n\pi y}{b}\right)\sin\left(\frac{n\pi y}{b}\right)dy=\frac{b}{2}$$

we arrive (with the sum contained in B_{mn}),

$$\sin\left(\frac{mnx'}{a}\right)\sin\left(\frac{n\pi y'}{b}\right)=\frac{ab}{4}B_{mn}. \quad \text{(A5)}$$

Thus, the first derivative respect to x,

$$\begin{aligned} \frac{\partial}{\partial x}G(x,z|x',z') &= \Gamma\sum_{m=0}^{\infty}\sum_{n=0}^{\infty}A_{mn}e^{\Gamma x}\sin\left(\frac{m\pi x}{a}\right)\sin\left(\frac{n\pi y}{b}\right) \\ &+\frac{mn}{a}\sum_{m=0}^{\infty}\sum_{n=0}^{\infty}A_{mn}e^{\Gamma x}\cos\left(\frac{m\pi x}{a}\right)\sin\left(\frac{n\pi y}{b}\right), \end{aligned} \quad \text{(A6)}$$

The second derivative,

$$\begin{aligned} &\frac{\partial^2 G}{\partial x^2}=\Gamma^2\sum_{m=0}^{\infty}\sum_{n=0}^{\infty}A_{mn}e^{\Gamma x}\sin\left(\frac{m\pi x}{a}\right)\sin\left(\frac{n\pi y}{b}\right)+\Gamma\frac{mn}{a}\sum_{m=0}^{\infty}\sum_{n=0}^{\infty}A_{mn}e^{\Gamma x}\cos\left(\frac{m\pi x}{a}\right)\sin\left(\frac{n\pi y}{b}\right) \\ &+\Gamma\sum_{m=0}^{\infty}\sum_{n=0}^{\infty}A_{mn}e^{\Gamma x}\cos\left(\frac{m\pi x}{a}\right)\sin\left(\frac{n\pi y}{b}\right)-\left(\frac{mn}{\omega}\right)^2\sum_{m=0}^{\infty}\sum_{n=0}^{\infty}A_{mn}e^{\Gamma x}\sin\left(\frac{m\pi x}{a}\right)\sin\left(\frac{n\pi y}{b}\right). \end{aligned} \quad \text{(A7)}$$

The first derivative respect to y,

$$\frac{\partial G}{\partial y}=\frac{n\pi}{b}\sum_{m=0}^{\infty}\sum_{n=0}^{\infty}A_{mn}e^{\Gamma x}\sin\left(\frac{m\pi x}{a}\right)\cos\left(\frac{n\pi y}{b}\right) \quad \text{(A8)}$$

The second derivative respect to y,

$$\frac{\partial^2 G}{\partial y^2} = -\left(\frac{n\pi}{b}\right)^2 \sum_{m=0}^{\infty}\sum_{n=0}^{\infty} A_{mn} e^{\Gamma x} \sin\left(\frac{m\pi x}{a}\right)\sin\left(\frac{n\pi y}{b}\right) \tag{A9}$$

Substituting into the Green equation, yields

$$\begin{aligned}
&\Gamma^2 \sum_{m=0}^{\infty}\sum_{n=0}^{\infty} A_{mn} e^{\Gamma x} \sin\left(\frac{m\pi x}{a}\right)\sin\left(\frac{n\pi y}{b}\right) + \Gamma \frac{mn}{a} \sum_{m=0}^{\infty}\sum_{n=0}^{\infty} A_{mn} e^{\Gamma x} \cos\left(\frac{m\pi x}{a}\right)\sin\left(\frac{n\pi y}{b}\right) \\
&+\Gamma \sum_{m=0}^{\infty}\sum_{n=0}^{\infty} A_{mn} e^{\Gamma x} \cos\left(\frac{m\pi x}{a}\right)\sin\left(\frac{n\pi y}{b}\right) - \left(\frac{mn}{\omega}\right)^2 \sum_{m=0}^{\infty}\sum_{n=0}^{\infty} A_{mn} e^{\Gamma x} \sin\left(\frac{m\pi x}{a}\right)\sin\left(\frac{n\pi y}{b}\right) \\
&-\left(\frac{n\pi}{b}\right)^2 \sum_{m=0}^{\infty}\sum_{n=0}^{\infty} A_{mn} e^{\Gamma x} \sin\left(\frac{m\pi x}{a}\right)\sin\left(\frac{n\pi y}{b}\right) + \Gamma^2 \sum_{m=0}^{\infty}\sum_{n=0}^{\infty} A_{mn} e^{\Gamma x} \sin\left(\frac{m\pi x}{a}\right)\sin\left(\frac{n\pi y}{b}\right) \\
&+\frac{mn}{a}\Gamma \sum_{m=0}^{\infty}\sum_{n=0}^{\infty} A_{mn} e^{\Gamma x} \cos\left(\frac{m\pi x}{a}\right)\sin\left(\frac{n\pi y}{b}\right) = -4\pi \sum_{m=0}^{\infty}\sum_{n=0}^{\infty} B_{mn} \sin\left(\frac{mnx}{a}\right)\sin\left(\frac{n\pi z}{b}\right),
\end{aligned} \tag{A10}$$

Collecting for A_{mn} and substituting A5, gives,

$$\begin{aligned}
&\sum_{m=0}^{\infty}\sum_{n=0}^{\infty} A_{mn} C e^{\Gamma x} \sin\left(\frac{m\pi x}{a}\right)\sin\left(\frac{n\pi y}{b}\right) + \sum_{m=0}^{\infty}\sum_{n=0}^{\infty} A_{mn} D e^{\Gamma x} \cos\left(\frac{m\pi x}{a}\right)\sin\left(\frac{n\pi y}{b}\right) = \\
&-4\pi \sum_{m=0}^{\infty}\sum_{n=0}^{\infty} \frac{4}{ab} \sin\left(\frac{mnx'}{a}\right)\sin\left(\frac{n\pi y'}{b}\right)\sin\left(\frac{mnx}{a}\right)\sin\left(\frac{n\pi z}{b}\right),
\end{aligned} \tag{A11}$$

with

$$C = \left[2\Gamma^2 - \left(\frac{m\pi}{a}\right)^2 - \left(\frac{n\pi}{b}\right)^2\right] \quad , \quad D = \left[2\Gamma \frac{mn}{a} + \Gamma\right]. \tag{A12}$$

Collecting for A_{mn}, we get,

$$\sum_{m=0}^{\infty}\sum_{n=0}^{\infty} A_{mn} e^{\Gamma x}\left[C \sin\left(\frac{m\pi x}{a}\right) + D\cos\left(\frac{m\pi x}{a}\right)\right] = -4\pi \sum_{m=0}^{\infty}\sum_{n=0}^{\infty} \frac{4}{ab} \sin\left(\frac{mnx'}{a}\right)\sin\left(\frac{n\pi y'}{b}\right)\sin\left(\frac{mnx}{a}\right),$$

……(A13)

Thus, solving for A_{mn}, yields

$$A_{mn} = -\frac{16}{ab} e^{-\Gamma x} \frac{\sin\left(\frac{mnx'}{a}\right)\sin\left(\frac{n\pi y'}{b}\right)\sin\left(\frac{mnx}{a}\right)}{\left[C \sin\left(\frac{m\pi x}{a}\right) + D\cos\left(\frac{m\pi x}{a}\right)\right]}. \tag{A14}$$

Finally we obtain the complete Green's function as follow,

$$G\left(x, y \middle| x', y'\right) = -\frac{16}{ab} \sum_{m=0}^{\infty}\sum_{n=0}^{\infty} \frac{\sin^2\left(\frac{m\pi x}{a}\right)\sin\left(\frac{n\pi y}{b}\right)}{\left[C \sin\left(\frac{m\pi x}{a}\right) + D\cos\left(\frac{m\pi x}{a}\right)\right]} \sin\left(\frac{m\pi x'}{a}\right)\sin\left(\frac{n\pi y'}{b}\right), \tag{A15}$$